# Amorphous Kane-Mele model in disordered hyperuniform two-dimensional networks

Junyan Ma [1] and Huaqing Huang [1,2,3,*]

[1]*School of Physics, Peking University, Beijing 100871, China*
[2]*Collaborative Innovation Center of Quantum Matter, Beijing 100871, China*
[3]*Center for High Energy Physics, Peking University, Beijing 100871, China*

(Received 11 September 2022; revised 30 October 2022; accepted 14 November 2022; published 28 November 2022)

As a prototype system of the quantum spin Hall effect, the Kane-Mele model which was proposed initially in graphene promotes the search for two-dimensional topological materials of hexagonal lattices. Here we generalize the Kane-Mele model to exotic amorphous systems which possess a remarkable structural property called hyperuniformity. We show that, in general, the Quantum spin Hall state still survives in disordered hyperuniform lattices that are constructed by structural transformation involving Stone-Wales defects. However, compared to that in the honeycomb lattice, the gapped topological region in the phase diagram shrinks and the size of the corresponding topological gap decreases remarkably in disordered hyperuniform lattices. By introducing random vacancies in either perfectly ordered or disordered hyperuniform lattices, we further show that the degradation or destruction of hyperuniformity is detrimental to the existence of gapped topological states. We therefore propose that the hyperuniform metric of an amorphous lattice, which quantifies the extent of disordered hyperuniformity, reflects its ability to preserve topological states. Our finding not only establishes the possible underlying link between electronic topology and disordered hyperuniformity but also provides useful guidance for the seeking of topological materials in amorphous states of matter.

DOI: 10.1103/PhysRevB.106.195150

## I. INTRODUCTION

Quantum spin Hall (QSH) effects, which are characterized by topological protected helical edge states within the insulating bulk gap, have attracted tremendous attention in the past decade [1–3]. So far, a large number of QSH materials have been discovered [4,5], most of them are based on two prevailing lattice models, i.e., the Bernevig-Hughes-Zhang (BHZ) [6] and Kane-Mele (KM) models [7,8]. The former was initially derived from the HgTe/CdTe quantum well system, where an inverted band order between valence and conduction bands with opposite parities occurs at the Γ point of the Brillouin zone [6]. On the other hand, the KM model starts from a Dirac semimetal of a hexagonal lattice such as graphene, where the valence and conduction bands touch each other to form a Dirac cone as a consequence of the hexagonal symmetry. As the band order has already been inverted in this case, any finite spin-orbit coupling (SOC) lifts the band degeneracy and opens a nontrivial SOC gap to turn the system into a QSH state [7,8]. Consequently, it triggered extensive research on other two-dimensional (2D) QSH materials of hexagonal lattices with large SOC, such as silicene, germanene, stanene, and their derivatives [9–11]. In addition, the two original models also inspired further research on the interplay of topological band structure and many-body interaction effects, such as Hubbard repulsion [12–14], Anderson localization [15–17], and quantum magnetism [18–20].

Stimulated by the rapid progress in the search for QSH states in crystalline materials, the study of topological phases has lately extended to noncrystalline solids [21,22]. Meanwhile, some novel topological states, such as the exotic phase of topological amorphous metal [23] and structural-disorder induced higher-order topological phases [24,25], have been predicted in amorphous systems. Recently, QSH states were proposed in quasicrystals [26–28] and amorphous lattices [29–34] based on the BHZ model with a band inversion mechanism. However, as the basic line of argument for constructing the KM model is reliant on the hexagonal lattice, it seems that the KM model cannot extend to amorphous systems where lattice symmetries are broken. In the course of searching for new amorphous topological materials, the following question naturally arose: Is it possible to realize the QSH state in amorphous lattices based on the KM model? If so, which type of structural disorder prefers to sustain rather than ruin the topological states?

We note that the recently proposed concept of hyperuniformity generalizes the traditional long-range order in many-particle systems to not only include crystals and quasicrystals but also some exotic amorphous systems [35–38]. Hyperuniform (or superhomogeneous) states of matter are characterized by an anomalously large suppression of long-wavelength (i.e., large length scale) density fluctuations, which indicates that the static structure factor $S(\mathbf{k})$ tends to zero as the wave number $k \equiv |\mathbf{k}|$ tends to zero, i.e., $\lim_{k\to 0} S(\mathbf{k}) = 0$. Disordered hyperuniform materials are special amorphous states of matter that lie between liquids and crystals. They are statistically isotropic without Bragg peaks like liquids or glasses, and yet they completely suppress

*huaqing.huang@pku.edu.cn

 

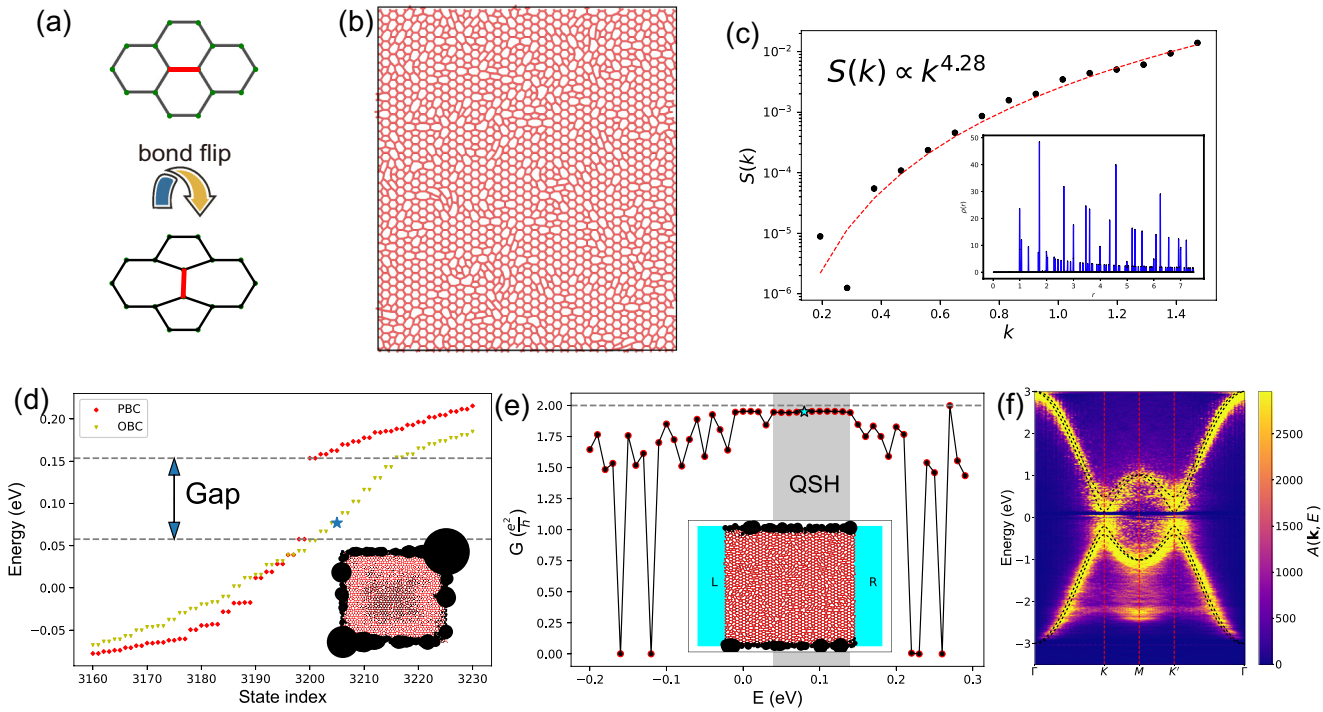


FIG. 1. (a) Schematic illustration of the bond flip process to form a SW defect. (b) A typical amorphous lattice of $p_{\mathrm{SW}} = 0.06$ (containing 3200 atoms); red lines indicate interatomic hoppings. (c) Structural factor $S(k)$ of the amorphous lattice converges to zero as the wave vector $k$ approaches zero, indicating the preservation of the disordered hyperuniformity. The inset shows the pair correlation function $\rho(r)$ of the amorphous lattice, where the distance is scaled by the bond length of the original honeycomb lattice. (d) The energy spectrum of the amorphous KM model in an disordered hyperuniform lattice with $p_{\mathrm{SW}} = 0.06$. The parameters used here are $\lambda_R = 0.05$, $\lambda_S = 0.06$, and $\lambda_v = 0.1$ eV [marked as red square in Fig. 2(a)]. The inset shows the real-space distribution of a midgap state [marked as blue asterisk in (d)]. (e) Two-terminal conductance $G$ as a function of the Fermi energy $E$. The inset shows the local density of state at $E = 0.08$ eV [marked as cyan asterisk in (e)] for the central amorphous sample. (f) Unfolded band structure of the amorphous KM model in the disordered hyperuniform structure, where the black dash lines indicate the bands of the pristine KM model with the same parameters in the honeycomb lattice.

large-scale density fluctuations similar to perfect crystals. Due to the hidden order on large length scales, disordered hyperuniform systems are endowed with novel physical properties and attract considerable attention [39–48]. Recently, Zheng *et al.* [49] reported the discovery of disordered hyperuniformity in 2D amorphous silica. Later, Chen *et al.* [50] showed that Stone-Wales (SW) defects (i.e., a typical topological defect composed of twinned pentagon-heptagon pairs in honeycomb lattices) [51] preserve hyperuniformity in 2D hexagonal structures, which are verified by recently synthesized amorphous graphene [52].

In view of the recent progress in topological physics and disordered hyperuniformity, here we generalize the KM model to amorphous 2D lattices with disordered hyperuniformity. Specifically, we construct the disordered hyperuniform lattices by continuously performing hyperuniformity-preserving SW transformations in 2D hexagonal network structures. Then we consider a modified KM model where the hopping integrals depend on intersite distances in the disordered hyperuniform lattice. The existence of QSH states is confirmed by numerical calculations and the topological phase diagrams in different parameter spaces are studied in depth. Finally, we investigate the effect of the degradation of hyperuniformity by introducing random vacancies in either perfectly ordered or disordered hyperuniform lattices and find that the degree of disordered hyperuniformity reflects the ability of the amorphous lattice to preserve the gapped topological state.

The organization of this paper is as follows. In Sec. II, we describe the model and method, including the construction of the disordered hyperuniform lattice, the amorphous KM model, the calculation of the spin Bott index, and unfolded band structure, and transport simulation based on the nonequilibrium Green's function (NEGF) formalism. In Sec. III, we identify the QSH state in disordered hyperuniform lattices and study the topological phase diagram of the amorphous KM model. Finally, we summarize our main conclusions in Sec. IV.

## II. MODEL AND METHOD

### A. Construction of the amorphous lattices

We construct amorphous lattices following the bond-flipping procedure, which has been proved to be an effective approach for generating hyperuniform 2D networks [49,50,53]. Specifically, starting from a pristine honeycomb lattice, we randomly select a certain number of bonds and rotate each bond by 90º, which changes its local network topology of the original honeycomb lattice, as shown in the inset of Fig. 1(a). The resulting defective local structures containing flipped bonds are composed of two pentagons and two heptagons, which are typically referred to as the SW defects.

After the bond-flipping procedure, all structures are optimized by molecular dynamics simulations using LAMMPS with the modified reactive empirical bond order potential [54]. The SW transformation generates amorphous lattices with fixed coordination numbers, which is a realistic feature of covalently bonded amorphous solids. In fact, it was previously known that SW defects preserve hyperuniformity in the amorphous 2D networks [49,50]. The concentration of SW defects $p_{\rm SW}$ is estimated as the fraction of bonds in the network that undergoes the SW transformation (i.e., $p_{\rm SW} \equiv N_{\rm SW}/N_b$, where $N_{\rm SW}$ is the number of SW transformations performed and $N_b$ is the number of bonds in the network). For comparison, we also construct disordered lattices with vacancies by randomly removing a certain number of atoms $N_v$. Similarly, the concentration of vacancies $p_v = N_v/N_a$ is defined as the ratio between $N_v$ and the total number of atoms $N_a$ in the lattice.

### B. Amorphous KM model

Due to the different bond length in the amorphous lattices, we modify the KM model [7,8] by considering the distance dependence of intersite hoppings which follows the Harrison's $r^{-2}$ scaling law [55]. The tight-binding (TB) Hamiltonian of the modified KM model for amorphous lattices is given by

$$H = \frac{d_0^2}{d_{ij}^2} t \sum_{\langle ij\rangle} c_i^\dagger c_j + i\lambda_R \sum_{\langle ij\rangle} c_i^\dagger (\boldsymbol{s}\times\hat{\mathbf{d}}_{ij})_z c_j, \\ + i\lambda_S \sum_{\langle\langle ij\rangle\rangle} v_{ij} c_i^\dagger s_z c_j + \lambda_v \sum_i \xi_i c_i^\dagger c_i, \tag{1}$$

where $c_i^\dagger (c_i)$ is a creation (annihilation) operator on site $i$. $t$ is the original spin-independent nearest neighbor (NN) hopping, which is set to 1 eV for simplicity. The single and double brackets $\langle\cdot\rangle/\langle\langle\cdot\rangle\rangle$ in summation run over all the NN or next-NN (NNN) hopping sites. $d_{ij} = |\mathbf{d}_{ij}|$ and $\hat{\mathbf{d}}_{ij} = \mathbf{d}_{ij}/d_{ij}$ are the length and unit vector of $\mathbf{d}_{ij}$, which is the NN vector from the site $i$ to $j$. Note that all lengths are scaled in units of the pristine bond length $d_0$ of the honeycomb lattice, and we set $d_0 = 1$ without loss of generality. $v_{ij} = (2/\sqrt{3})(\hat{\mathbf{d}}_{ik}\times\hat{\mathbf{d}}_{kj})$, where site $k$ connects the NNN sites $i$ and $j$. $\boldsymbol{s} = (s_x, s_y, s_z)$ are the Pauli matrices for the spin degree of freedom. $\lambda_R$ and $\lambda_S$ are the strength of the Rashba and intrinsic SOC, respectively. The last term is a staggered potential with $\xi_i = \pm 1$ indicating the original A and B sublattices. Noting that the staggered potentials is absence for elemental substances such as graphene [56], silicene [9,57], germanene [10,58], and stanane [11], we also discuss the amorphous KM model without the staggered potential ($\lambda_v = 0$), as presented in the Supplemental Material [59].

### C. Spin Bott index

To verify the bulk topology of the amorphous KM model, we compute the real-space topological invariant, the spin Bott index $B_s$, which enables the identification of quantum spin Hall (QSH) states in both crystalline and noncrystalline systems [26,27]. To obtain the spin Bott index $B_s$, we first split all eigenstates into two spin subspaces according to their expectation values of $s_z$. Specifically, we solve the eigenvalue problem for the projected spin operator,

$$P_z|\phi_\pm^i\rangle = s_\pm^i|\phi_\pm^i\rangle, \tag{2}$$

where $P_z = Ps_zP$, and $P = \sum_{J\in\rm occ}|\psi_J\rangle\langle\psi_J|$ is the projector operator of the occupied states. The subscript $\pm$ stands for the sign of eigenvalues. Apart from some irrelevant zero eigenvalues, $s_\pm^i$ are equal to $\pm 1$ precisely for systems with spin $s_z$ conservation. For systems with spin-mixing terms (e.g., the nonzero Rashba SOC), $s_\pm^i$ deviates from $\pm 1$. In this case, we can still construct the projected position operators for two subspaces with opposite signs of $s_\pm^i$, respectively,

$$U_\pm = P_\pm e^{i2\pi X}P_\pm + Q_\pm, \quad V_\pm = P_\pm e^{i2\pi Y}P_\pm + Q_\pm, \tag{3}$$

where $P_\pm = I - Q_\pm = \sum_i |\phi_\pm^i\rangle\langle\phi_\pm^i|$ is the projector to occupied states of spin $\pm$, and $X, Y$ are the normalized coordinates defined between [0,1). Finally, we calculate the Bott index for each spin

$$B_\pm = \frac{1}{2\pi}\mathrm{Im}\{\mathrm{tr}[\ln(V_\pm U_\pm V_\pm^\dagger U_\pm^\dagger)]\} \tag{4}$$

and obtain the spin Bott index as $B_s = (B_+ - B_-)/2$. Similar to the nontrivial $Z_2$ topological invariant which represents an obstruction for the construction of Wannier functions with a smooth gauge that respects the time-reversal symmetry [60], the nonzero spin Bott index also indicates the topological obstruction to construct exponentially localized Wannier functions. Thus, it identifies the nontrivial topology of the occupied states. The effectiveness and robustness are guaranteed by the insulating gap of the Hamiltonian and the spectral gap of the projected spin operator $P_z$ [27].

### D. Unfolded band structure of amorphous lattices

To directly compare the band structures of a pristine honeycomb lattice and amorphous lattice, we construct an effective band structure for the amorphous KM model from a supercell calculation using the band-unfolding method [61–64]. Since the amorphous lattice is usually studied based on supercell calculations with an artificial periodic boundary condition, here we use upper and lower case symbols to define variables corresponding to the supercell and primitive cell. For example, $\mathbf{K}$, $\mathbf{R}$, and $N$ ($\mathbf{k}$, $\mathbf{r}$, and $n$) represent the crystal momentum, the lattice vector, and the index of orbitals for the supercell (primitive cell). According to the scheme of linear combination of atomic orbitals (LCAO), the $J$th supercell Bloch state at $\mathbf{K}$ can be expanded under the atomic basis function $\{|\mathbf{R}+\mathbf{t}_N, N, \sigma\rangle\}$ as

$$|\mathbf{K}, J\rangle = \sum_{N,\sigma} C_{N,\sigma}^{\mathbf{K},J} \sum_{\mathbf{R}} e^{i\mathbf{K}\cdot(\mathbf{R}+\mathbf{t}_N)}|\mathbf{R}+\mathbf{t}_N, N, \sigma\rangle, \tag{5}$$

where $\mathbf{t}_N$ is the location of orbital $N$ in the supercell and $\sigma$ denotes spin up and spin down. We obtain the LCAO coefficient $C_{N,\sigma}^{\mathbf{K},J}$ by directly diagonalizing Eq. (1) at a given $\mathbf{K}$. Because the notation of a basis function $|\mathbf{R}, N, \sigma\rangle$ in the supercell is the equivalence of $|\mathbf{R}+\mathbf{r}(N,\sigma), n(N,\sigma), \sigma\rangle$ in a primitive cell under the TB approximation [63], the unfolded spectral weight can be written as [65]

$$W^{\mathbf{K},J}(\mathbf{k}) = \sum_{M,\sigma',N,\sigma} \tilde{C}_{N,\sigma}^{\mathbf{K},J} C_{M,\sigma'}^{\mathbf{K},J} e^{i\mathbf{k}\cdot[\mathbf{r}(N,\sigma)-\mathbf{r}(M,\sigma')]}. \tag{6}$$

Finally, we obtain the spectral function at a specific energy $E$ and primitive crystal momentum $\mathbf{k}$ as

$$A(\mathbf{k}, E) = \sum_{\mathbf{K},J} W^{\mathbf{K},J}(\mathbf{k})\delta(E - E_{\mathbf{K},J}), \tag{7}$$

where $E_{\mathbf{K},J}$ is the eigenenergy of band $J$ at $\mathbf{K}$ [64,66]. For the amorphous KM model, we construct supercells containing over 3200 sites, the corresponding first Brillouin zone is so tiny that only a single $\Gamma$ point is adopted in the supercell calculation.

### E. Transport simulations based on NEGF method

As an important consequence of the bulk topology, the existence of topological edge states leads to quantized charge conductance [8]. We investigate the transport properties of the amorphous lattice based on the nonequilibrium Green's function method [67–71]. In the transport simulation, a finite amorphous sample is coupled to two semi-infinite leads, which can be broken down into periodic stacks of principal layers. For simplicity, the principal layer is set the same as the central part. and the interlayer couplings are determined using the periodic boundary condition along the transport direction and the open boundary condition in the perpendicular direction.

## III. RESULTS

### A. Disordered hyperuniform lattice

According to previous studies [50], disordered hyperuniformity is preserved in the amorphous lattice as long as the SW defect concentration $p_{\mathrm{SW}} \leqslant 0.14$. As a first attempt, we investigate the amorphous KM model in the disordered hyperuniform 2D lattice with a fixed $p_{\mathrm{SW}} = 0.06$. We present a typical configuration of the amorphous lattice with $p_{\mathrm{SW}} = 0.06$ in Fig. 1(b). Since hyperuniform systems can be characterized by a structure factor $S(k)$ with a radial power-law form $S(k) \sim |\mathbf{k}|^{\alpha}$ in the vicinity of the origin [36], we plot the $S(k)$ for the amorphous lattice, as shown in Fig. 1(c). The structural factor $S(k)$ goes to 0 with scaling exponent $\alpha \approx 4.28$ in the limit $k \to 0$, indicating the preservation of class I ($\alpha > 1$) disordered hyperuniformity [35,48,72]. Moreover, as shown in the inset of Fig. 1(c), the pair correlation function $\rho(r)$ exhibits sharp peaks at isolated distances, indicating that local structural characteristics, such as the average bond length, are similar to their crystalline counterparts.

### B. Topological state in disordered hyperuniform lattices

As an illustrative example of the QSH state in the disordered hyperuniform lattice, we present the detailed results of the amorphous KM model with fixed parameters $\lambda_R = 0.05$, $\lambda_S = 0.06$, and $\lambda_v = 0.1$ eV in Figs. 1(d)–1(f). For the disordered hyperuniform lattice shown in Fig. 1(b), the calculated energy spectrum with an artificial periodic boundary condition (PBC) shows an energy gap, indicating that the system is an insulator. When an open boundary condition (OBC) is adopted, a set of edge states, as expected, appears in pairs in the gap region. Moreover, these states are localized on the edges of the finite amorphous sample [see inset in Fig. 1(d)], which coincides with the nontrivial topology characterized by the nonzero spin Bott index ($B_s = 1$).

We also verify the conductive feature of these topological edge states by directly calculating the two-terminal conductance based on the NEGF method. As shown in Fig. 1(e), there is a nearly quantized conductance of $G = 2e^2/h$ in the gap region of the energy spectrum, indicating the nontrivial bulk topology. Moreover, the conductive channels of the quantized plateau are mainly contributed by the topological edge states, which is verified by the real-space distribution of the local density of states for the central amorphous lattice at $E = 0.08$ eV [see inset of Fig. 1(e)]. As the edge states are not eigenstates of the perpendicular component of the spin, $s_z$, due to the existence of the Rashba SOC, the spin Hall conductances are not necessarily quantized. However, nonzero spin accumulation persists at the edge when topological edge states cross the Fermi level $E_F$ [7].

To directly examine the effect of structural amorphization on the band structure, we unfold the energy spectrum of the amorphous KM model into the primitive Brillouin zone of the intrinsic honeycomb lattice. As shown in Fig. 1(f), the unfolded band structure of the amorphous lattice retains the overall band shape of the pristine KM model on the intrinsic honeycomb lattice (black dash lines). However, SW defects cause smearing and breaking up of the unfolded bands, which reflects a finite lifetime of the quasiparticles in the amorphous lattice. It is also worthy noting that SW defects give rise to extra defect states, which forms new flat bands, around the conduction band minimum and valence band maximum [65,73]. Due to the broadening of the spectral functions and the emergence of defect states, the effective energy gap of the amorphous lattice decreases. It is, therefore, expected that the energy gap would diminish gradually with the increasing concentration of SW defects, as discussed later.

### C. Phase diagram of the amorphous KM model

According to the pioneering work of Kane and Mele [7], there is a clean phase boundary [marked as the black dotted line in Figs. 2(a) and 2(b)] between the QSH and normal insulator when $\lambda_R/\lambda_S < 2\sqrt{3}$ and $\lambda_v/\lambda_S < 3\sqrt{3}$. To determine the phase diagram of the amorphous KM model, all physical quantities, such as the energy gap and spin Bott index, are calculated with the configuration average of over 50 realizations of amorphous lattices for a given $p_{\mathrm{SW}}$. Figures 2(a) and 2(b) show the phase diagram of the amorphous KM model in the $(\lambda_R/\lambda_S, \lambda_v/\lambda_S)$ parameter space with a fixed $\lambda_S = 0.06$ eV in accordance with Ref. [7]. For the amorphous KM model, the QSH state is separate from a gapless state (instead of a normal insulator for the pristine KM model) by a curved phase boundary [the red dashed line in Fig. 2(a)], although a normal insulator state would eventually appear at a large value of $\lambda_v/\lambda_S$ (>10, not shown here). It is noted that the topologically nontrivial states of the amorphous and pristine KM models share a similar area in the phase diagram, which suggests the robust survivability of the QSH state in amorphous systems. As shown in Fig. 2(b), the distribution of $B_s$ is compatible with the evolution of the energy gap in Fig. 2(a), despite a slight discrepancy in the phase boundary due to the numerical inefficiency for systems with small gaps.

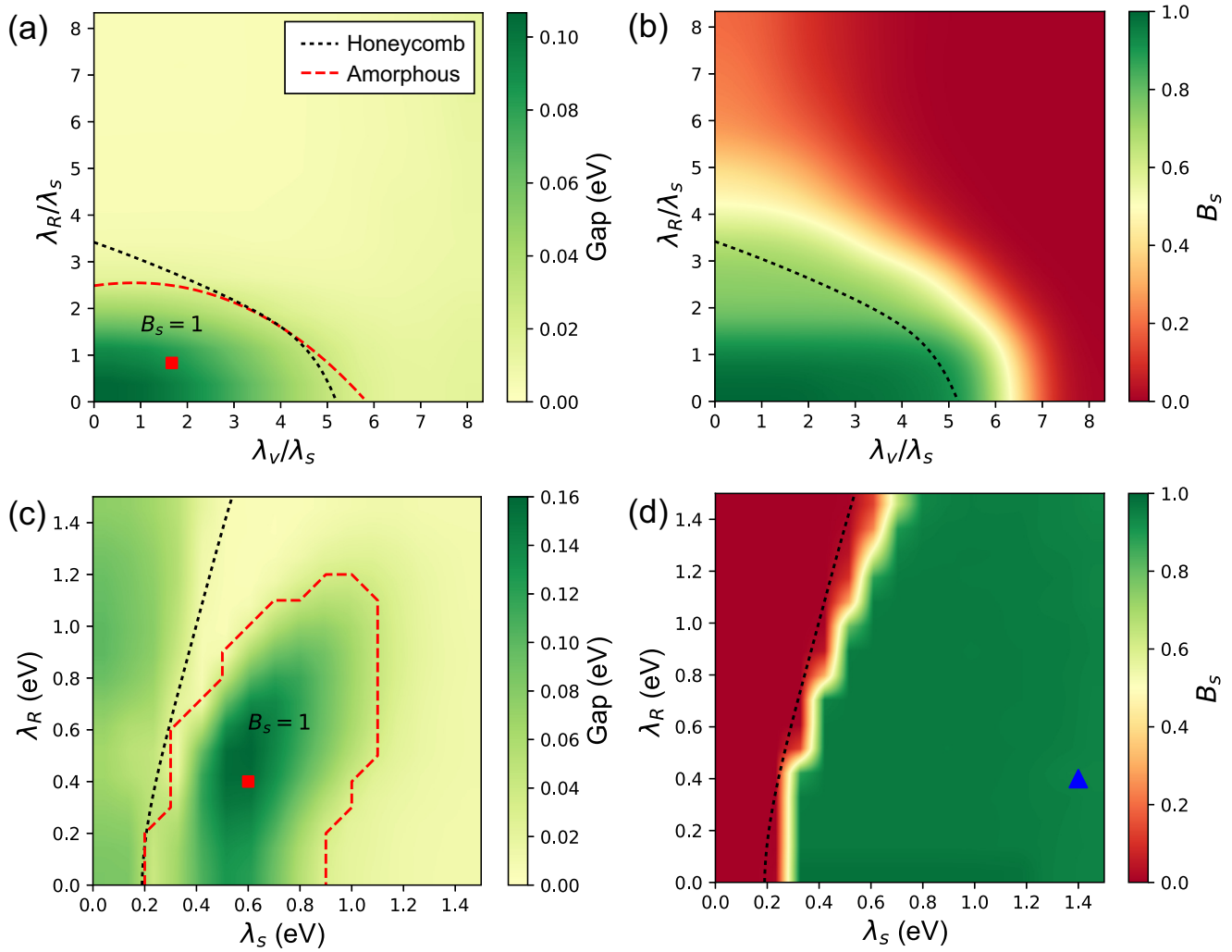


FIG. 2. (a), (b) The distribution of (a) energy gap and (b) spin Bott index in the ($\lambda_R/\lambda_S$, $\lambda_v/\lambda_S$) parameter space of the amorphous KM model on the disordered hyperuniform lattice with $p_{\mathrm{SW}} = 0.06$. (c), (d) The distribution of (c) energy gap and (d) spin Bott index in the $\lambda_R$-$\lambda_S$ plane with fixed $\lambda_v = 1$ for the amorphous lattice. The black dotted line and red dashed line represent the gap-close boundary for the pristine honeycomb lattice and amorphous lattice, respectively. The red square point in (a) [(c)] represents the system shown in Fig. 1 (Fig. S1 in the Supplemental Material [59]). The blue up-pointing triangle in (d) stands for the system shown in Fig. S7 in the Supplemental Material [59].

This further confirms the topological phase in the amorphous lattice. However, the energy gaps of amorphous lattices are about one order of magnitude smaller than that of pristine ones under the same TB parameters (see Fig. 3(a) and Fig. S1 in the Supplemental Material [59]), implying a strong effect of structural amorphization on the electronic topology.

Next, we study the phase evolution of pristine and amorphous KM models with a fixed staggered potential $\lambda_v = 1$ eV. Figures 2(c) and 2(d) show the phase diagram in the $\lambda_R$-$\lambda_S$ plane. For the pristine KM model on the honeycomb lattice, the QSH and normal insulator phases are divided by an energy gap closing line, which is plotted as the black dotted line in Figs. 2(c) and 2(d). On the contrary, for the amorphous KM model, only a small region [the area surrounded by the red dashed line in Fig. 2(c)] remains to be the QSH insulator with a finite gap. The energy gap decreases dramatically to almost zero with either increasing of $\lambda_R$ or $\lambda_S$, as shown in Fig. 2(c). Because both the Rashba and intrinsic SOC terms depend on local atomic environments (i.e., the relative bond orientations $\hat{\mathbf{d}}_{ij}$), the effect of structural amorphization becomes more important when $\lambda_R$ and $\lambda_S$ dominate the spectral gap. Remarkably, as shown in Fig. 2(d), the phase boundary of the amorphous lattice from $B_s$ calculations is distinct from the gap-close boundary (red dashed line) in Fig. 2(c), but nearly coincides with that of the pristine model. This implies that the amorphous KM model highly preserves the topological properties as the pristine model. Comparing Figs. 2(c) and 2(d), one can find that there exists a gapless region with nonzero $B_s$ in the right of the phase diagram (e.g., when $\lambda_S > 1.2$). These states are dubbed gapless QSH insulators [74], which are characterized by the closed gap and nonzero spin Bott index. Both gapped and gapless QSH insulators manifest the nontrivial topology with robust topological edge states. Nevertheless, except for the edge states, the bulk states can also contribute to the electronic transport in gapless QSH insulators. Therefore, the electronic transport in gapless QSH insulators are not dissipationless and the conductances are no longer quantized (see Fig. S7 in Supplemental Material [59]). Thus, we focus on gapped QSH insulators which have more practical implications in potential applications.

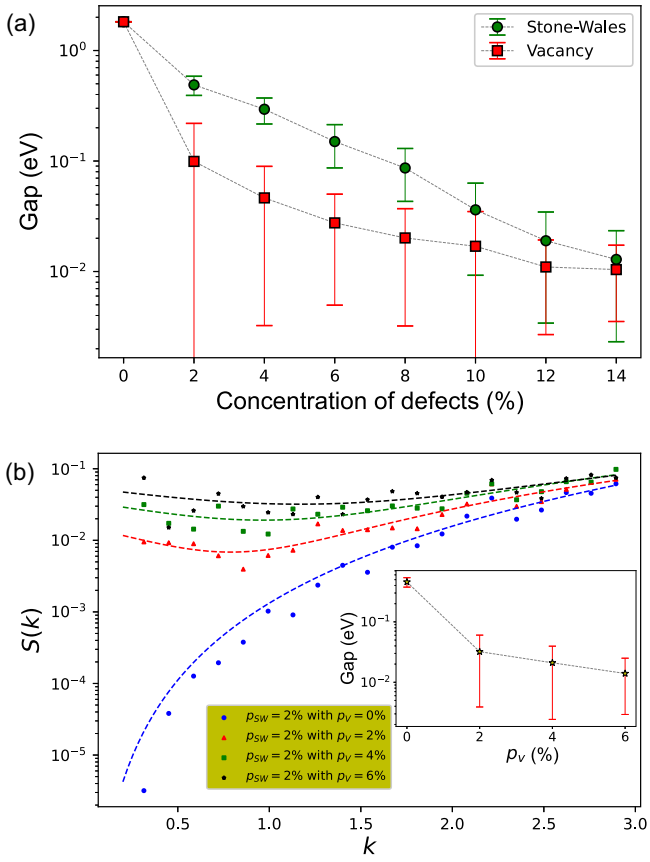


FIG. 3. (a) Semilog plots of the energy gap versus concentration of SW defects or vacancies. The parameters used here are $\lambda_R = 0.4$, $\lambda_S = 0.6$, and $\lambda_v = 1.0$ eV. (b) Structural factor $S(k)$ of amorphous lattices with SW defects and vacancies. The concentration of SW defects is fixed at $p_{SW} = 0.02$, while the concentration of vacancies varies from $p_v = 0$ to 0.06. The inset shows the energy gap of disordered systems in (b) with the same TB parameters used in (a).

In addition, we note that the normal insulator region in the phase diagram seems unaffected for the pristine and amorphous lattices. For the normal insulator phase in the left bottom region with small $\lambda_S$, the energy gap is mainly determined by the NN hopping term and the staggered potential. According to Eq. (1), the hopping term depends only on the NN coordination number (i.e., the number of NN sites) and average bond length [see the inset of Fig. 1(c)], while the staggered potential relies on the sublattice symmetry of the honeycomb lattice. As the local structural environment is fairly retained but lattice symmetries are broken in disordered hyperuniform lattices, the normal insulator with a reduced energy gap still preserves.

As a test, we also calculated disordered nonhyperuniform lattices [36] with the same coordination number but different distribution of bond lengths [75]. It is found that the normal insulator phase disappears from the phase diagram while the gapped QSH region remains (see Figs. S9 and S10 in the Supplemental Material [59]). Alternatively, by randomly removing NN bonds of a honeycomb lattice, one can reduce the average coordination number but keep the same bond length. Contrarily, the normal insulator phase remains and the gapped QSH state disappears completely in this case (see Fig. S11 in the Supplemental Material [59]). From the above calculations, we conclude that the topological state would generally still survive in amorphous lattices, although the gapped topological area in the parameter space shrinks significantly and the size of the corresponding topological gap is much smaller compared to the pristine KM model with the same parameters.

### D. Effect of defect types and concentrations

The above results suggest that the effect of structural amorphization to modify gapped topological states is triggered by a gap-closing mechanism. Then, one may expect the ability of disordered hyperuniform lattices to preserve the topological gap is dependent on the defect concentration $p_{SW}$; namely, the larger $p_{SW}$ is, the smaller the nontrivial energy gap will be. To reveal the dependence, we calculate the bulk energy gap as a function of $p_{SW}$. As shown in Fig. 3(a), with increasing $p_{SW}$, the topological energy gap decreases monotonically to nearly zero, implying the occurrence of gap closure. It is previously reported that introducing imperfections (such as vacancies) in perfectly ordered or disordered hyperuniform systems would degrade or destroy their original perfect hyperuniformity [76]. Therefore, we also consider disorder lattices with random vacancies [77,78]. Noting that vacancies in graphene induce midgap states which are mainly contributed by atoms nearest the vacancies [65,79], it is expected that the presence of random vacancies tends to reduce the topological gap. As shown in Fig. 3(a), the energy gap indeed decreases rapidly with the increasing vacancy concentration $p_v$.

Different from SW defects which preserve hyperuniformity in amorphous lattices [50], vacancies degrade hyperuniformity in proportion to the defect concentration $p_v$ [76], which leads to significant damage to the topological state. To analyze quantitatively the extent to which hyperuniformity is destroyed when vacancies are introduced, we calculate the hyperuniform metric [36,76],

$$\mathcal{H} = \frac{S(k \to 0)}{S(k_{\text{peak}})}, \tag{8}$$

where $S(k_{\text{peak}})$ is the structure factor at the first dominant peak. If the ratio $\mathcal{H}$ is of the order of $10^{-4}$ or smaller, the disordered system can be regarded as effectively hyperuniform, otherwise it is nonhyperuniform [36,76,80]. We study amorphous lattices with different vacancy concentrations $p_v$ and a fixed $p_{SW} = 0.02$. As shown in Fig. 3(b), the structural factor $S_0(k)$ of the amorphous lattice without vacancy ($p_v = 0$) vanishes rapidly as in the small-wave-vector limit, and the corresponding hyperuniform metric is $\mathcal{H} \sim 10^{-5}$. However, for amorphous lattices with a finite concentration of vacancies, the structural factor $S(k)$ converges to a nonzero value of the order of $10^{-2}$ in the limit $k \to 0$. Consequently, the hyperuniform metric $\mathcal{H}$ increases to the order of $10^{-1} \sim 10^{-2}$, indicating the nonhyperuniformity of these systems.

In addition, the vacancy-induced destruction of hyperuniformity also affects the topological gap. As shown in the inset of Fig. 3(b), the energy gap decreases further with the increase of $p_v$, implying that the degradation of hyperuniformity declines the ability to preserve bulk topology. Specifically, for the disordered hyperuniform lattice with $p_{SW} = 0.02$, a very

low concentration of vacancies (e.g., $p_v = 0.02$) would reduce the energy gap by more than 50%. And the resultant gap size is even smaller than that of disordered hyperuniform lattices with $p_{\mathrm{SW}} = 0.04$ and $p_v = 0$, indicating that vacancies are more detrimental to the topological gap than SW defects. When the concentration $p_v$ increases to 0.06, the energy gap reduces to be comparable with that of amorphous lattices with $p_{\mathrm{SW}} = 0.14$ in the absence of vacancies $p_v = 0$. Given the opposite trends of the topological gap and the hyperuniform metric $\mathcal{H}$ with the increasing concentration of vacancies $p_v$, we expect that $\mathcal{H}$ can signal the compatibility between the structural amorphization and topological states. To further strengthen our conclusion, we also investigate the relation between $\mathcal{H}$ and the topological gap at high concentrations of SW defects in the Supplemental Material [59].

## IV. CONCLUSION

In summary, we studied the amorphous KM model in disordered hyperuniform lattices which are constructed by performing SW transformations on the honeycomb lattice. In general, the QSH state survives in amorphous lattices with disordered hyperunformity. The resulting QSH phase is confirmed by the nonzero spin Bott index, robust edge states, and quantized conductance. With the increasing concentration of SW defects, the gapped topological region in the phase diagram shrinks gradually, associated with the decline of the topological energy gap. We also verify the existence of gapless QSH insulators which manifest a weak metallic behavior in amorphous networks, implying the impossibility of observation of stable quantized conductance in gapless states. In comparison, we also considered the degradation of hyperuniformity induced by random vacancies and found that the topological state vanishes rapidly after introducing vacancies in either perfectly ordered or disordered hyperuniform systems. We therefore expect that the hyperuniform metric $\mathcal{H}$ of amorphous lattices, which delineates the effective hyperuniformity, signals their ability to sustain topological states. As structural disorders are inevitable in the synthesis of realistic materials, our results point to the possible preservation of topological states in disordered hyperuniform materials, which largely release the high-quality constraint of preparing topological materials.

## ACKNOWLEDGMENTS

We thank Duyu Chen, Houlong Zhang, Yan Jiao, and Mohan Chen for valuable discussions. This paper was supported by the National Natural Science Foundation of China (Grant No. 12074006), the National Key R&D Program of China (No. 2021YFA1401600), and the startup fund from Peking University. The computational resources were supported by the high-performance computing platform of Peking University.

[1] M. Z. Hasan and C. L. Kane, Rev. Mod. Phys. **82**, 3045 (2010).
[2] X.-L. Qi and S.-C. Zhang, Rev. Mod. Phys. **83**, 1057 (2011).
[3] A. Bansil, H. Lin, and T. Das, Rev. Mod. Phys. **88**, 021004 (2016).
[4] H. Huang, Y. Xu, J. Wang, and W. Duan, WIRES: Comp. Mol. Sci. **7**, e1296 (2017).
[5] Z. Wang, K.-H. Jin, and F. Liu, WIRES: Comp. Mol. Sci. **7**, e1304 (2017).
[6] B. A. Bernevig, T. L. Hughes, and S.-C. Zhang, Science **314**, 1757 (2006).
[7] C. L. Kane and E. J. Mele, Phys. Rev. Lett. **95**, 146802 (2005).
[8] C. L. Kane and E. J. Mele, Phys. Rev. Lett. **95**, 226801 (2005).
[9] C.-C. Liu, W. Feng, and Y. Yao, Phys. Rev. Lett. **107**, 076802 (2011).
[10] C. Si, J. Liu, Y. Xu, J. Wu, B.-L. Gu, and W. Duan, Phys. Rev. B **89**, 115429 (2014).
[11] Y. Xu, B. Yan, H.-J. Zhang, J. Wang, G. Xu, P. Tang, W. Duan, and S.-C. Zhang, Phys. Rev. Lett. **111**, 136804 (2013).
[12] S. Raghu, X.-L. Qi, C. Honerkamp, and S.-C. Zhang, Phys. Rev. Lett. **100**, 156401 (2008).
[13] M. Dzero, K. Sun, V. Galitski, and P. Coleman, Phys. Rev. Lett. **104**, 106408 (2010).
[14] M. Hohenadler, T. C. Lang, and F. F. Assaad, Phys. Rev. Lett. **106**, 100403 (2011).
[15] J. Li, R.-L. Chu, J. K. Jain, and S.-Q. Shen, Phys. Rev. Lett. **102**, 136806 (2009).
[16] C. W. Groth, M. Wimmer, A. R. Akhmerov, J. Tworzydło, and C. W. J. Beenakker, Phys. Rev. Lett. **103**, 196805 (2009).
[17] C. P. Orth, T. Sekera, C. Bruder, and T. L. Schmidt, Sci. Rep. **6**, 24007 (2016).
[18] C.-X. Liu, X.-L. Qi, X. Dai, Z. Fang, and S.-C. Zhang, Phys. Rev. Lett. **101**, 146802 (2008).
[19] R. Yu, W. Zhang, H.-J. Zhang, S.-C. Zhang, X. Dai, and Z. Fang, Science **329**, 61 (2010).
[20] S. K. Kim, H. Ochoa, R. Zarzuela, and Y. Tserkovnyak, Phys. Rev. Lett. **117**, 227201 (2016).
[21] R. Zallen, *The Physics of Amorphous Solids* (John Wiley & Sons, Hoboken, New Jersey, 1998).
[22] V. Frechette, *Non-Crystalline Solids* (Wiley, New York, 1958).
[23] Y.-B. Yang, T. Qin, D.-L. Deng, L.-M. Duan, and Y. Xu, Phys. Rev. Lett. **123**, 076401 (2019).
[24] A. Agarwala, V. Juričić, and B. Roy, Phys. Rev. Res. **2**, 012067(R) (2020).
[25] J.-H. Wang, Y.-B. Yang, N. Dai, and Y. Xu, Phys. Rev. Lett. **126**, 206404 (2021).
[26] H. Huang and F. Liu, Phys. Rev. Lett. **121**, 126401 (2018).
[27] H. Huang and F. Liu, Phys. Rev. B **98**, 125130 (2018).
[28] H. Huang and F. Liu, Phys. Rev. B **100**, 085119 (2019).
[29] A. Agarwala and V. B. Shenoy, Phys. Rev. Lett. **118**, 236402 (2017).
[30] C. Wang, T. Cheng, Z. Liu, F. Liu, and H. Huang, Phys. Rev. Lett. **128**, 056401 (2022).
[31] M. Costa, G. R. Schleder, M. Buongiorno Nardelli, C. Lewenkopf, and A. Fazzio, Nano Lett. **19**, 8941 (2019).

[32] I. Sahlberg, A. Weststrom, K. Pöyhönen, and T. Ojanen, Phys. Rev. Res. **2**, 013053 (2020).

[33] P. Mukati, A. Agarwala, and S. Bhattacharjee, Phys. Rev. B **101**, 035142 (2020).

[34] G.-W. Chern, Europhys. Lett. **126**, 37002 (2019).

[35] S. Torquato and F. H. Stillinger, Phys. Rev. E **68**, 041113 (2003).

[36] S. Torquato, Phys. Rep. **745**, 1 (2018).

[37] C. E. Zachary and S. Torquato, J. Stat. Mech. Theory Exp. (2009) P12015.

[38] E. C. Oğuz, J. E. S. Socolar, P. J. Steinhardt, and S. Torquato, Phys. Rev. B **95**, 054119 (2017).

[39] O. U. Uche, F. H. Stillinger, and S. Torquato, Phys. Rev. E **70**, 046122 (2004).

[40] S. Torquato, G. Zhang, and F. H. Stillinger, Phys. Rev. X **5**, 021020 (2015).

[41] R. D. Batten, F. H. Stillinger, and S. Torquato, Phys. Rev. Lett. **103**, 050602 (2009).

[42] G. Zhang, F. H. Stillinger, and S. Torquato, J. Chem. Phys. **145**, 244109 (2016), .

[43] M. Florescu, S. Torquato, and P. J. Steinhardt, Proc. Natl. Acad. Sci. USA **106**, 20658 (2009).

[44] S. Yu, C.-W. Qiu, Y. Chong, S. Torquato, and N. Park, Nat. Rev. Mater. **6**, 226 (2021).

[45] D. Chen and S. Torquato, Acta Mater. **142**, 152 (2018).

[46] J. Kim and S. Torquato, Proc. Natl. Acad. Sci. USA **117**, 8764 (2020).

[47] J. Kim and S. Torquato, New J. Phys. **22**, 123050 (2020).

[48] S. Torquato and J. Kim, Phys. Rev. X **11**, 021002 (2021).

[49] Y. Zheng, L. Liu, H. Nan, Z.-X. Shen, G. Zhang, D. Chen, L. He, W. Xu, M. Chen, Y. Jiao *et al.*, Sci. Adv. **6**, eaba0826 (2020).

[50] D. Chen, Y. Zheng, L. Liu, G. Zhang, M. Chen, Y. Jiao, and H. Zhuang, Proc. Natl. Acad. Sci. USA **118**, e2016862118 (2021).

[51] A. Stone and D. Wales, Chem. Phys. Lett. **128**, 501 (1986).

[52] C.-T. Toh, H. Zhang, J. Lin, A. S. Mayorov, Y.-P. Wang, C. M. Orofeo, D. B. Ferry, H. Andersen, N. Kakenov, Z. Guo *et al.*, Nature (London) **577**, 199 (2020).

[53] M. A. Spencer and R. M. Ziff, Phys. Rev. E **93**, 042132 (2016).

[54] A. P. Thompson, H. M. Aktulga, R. Berger, D. S. Bolintineanu, W. M. Brown, P. S. Crozier, P. J. in 't Veld, A. Kohlmeyer, S. G. Moore, T. D. Nguyen, R. Shan, M. J. Stevens, J. Tranchida, C. Trott, and S. J. Plimpton, Comput. Phys. Commun. **271**, 108171 (2022).

[55] W. A. Harrison, *Electronic Structure and the Properties of Solids: The Physics of the Chemical Bond* (Courier Corporation, North Chelmsford, MA, 2012).

[56] Y. Yao, F. Ye, X.-L. Qi, S.-C. Zhang, and Z. Fang, Phys. Rev. B **75**, 041401(R) (2007).

[57] M. Ezawa, Phys. Rev. Lett. **109**, 055502 (2012).

[58] H. Pan, Z. Li, C.-C. Liu, G. Zhu, Z. Qiao, and Y. Yao, Phys. Rev. Lett. **112**, 106802 (2014).

[59] See Supplemental Material at http://link.aps.org/supplemental/10.1103/PhysRevB.106.195150 for more details about numerical results with different parameters and the topological properties of the amorphous KM model in other nonhyperuniform lattices.

[60] A. A. Soluyanov and D. Vanderbilt, Phys. Rev. B **83**, 035108 (2011).

[61] H. Huang, F. Zheng, P. Zhang, J. Wu, B.-L. Gu, and W. Duan, New J. Phys. **16**, 033034 (2014).

[62] V. Popescu and A. Zunger, Phys. Rev. B **85**, 085201 (2012).

[63] C.-C. Lee, Y. Yamada-Takamura, and T. Ozaki, J. Phys.: Condens. Matter **25**, 345501 (2013).

[64] H. Nishi, Y.-i. Matsushita, and A. Oshiyama, Phys. Rev. B **95**, 085420 (2017).

[65] M. Farjam, J. Phys. Condens. Matter. **26**, 155502 (2014).

[66] P. B. Allen, T. Berlijn, D. A. Casavant, and J. M. Soler, Phys. Rev. B **87**, 085322 (2013).

[67] M. Büttiker, Phys. Rev. B **38**, 9375 (1988).

[68] F. Guinea, C. Tejedor, F. Flores, and E. Louis, Phys. Rev. B **28**, 4397 (1983).

[69] A. H. Larsen, J. J. Mortensen, J. Blomqvist, I. E. Castelli, R. Christensen, M. Dułak, J. Friis, M. N. Groves, B. Hammer, C. Hargus, E. D. Hermes, P. C. Jennings, P. B. Jensen, J. Kermode, J. R. Kitchin, E. L. Kolsbjerg, J. Kubal, K. Kaasbjerg, S. Lysgaard, J. B. Maronsson *et al.*, J. Phys.: Condens. Matter **29**, 273002 (2017).

[70] H. Huang, Z. Wang, N. Luo, Z. Liu, R. Lü, J. Wu, and W. Duan, Phys. Rev. B **92**, 075138 (2015).

[71] S. Datta, *Electronic Transport in Mesoscopic Systems* (Cambridge University Press, Cambridge, England, 1997).

[72] S. Torquato, A. Scardicchio, and C. E. Zachary, J. Stat. Mech. Theory Exp. (2008) P11019.

[73] P. V. C. Medeiros, S. Stafström, and J. Björk, Phys. Rev. B **89**, 041407(R) (2014).

[74] M. Gonçalves, P. Ribeiro, R. Mondaini, and E. V. Castro, Phys. Rev. Lett. **122**, 126601 (2019).

[75] P. N. Keating, Phys. Rev. **145**, 637 (1966).

[76] J. Kim and S. Torquato, Phys. Rev. B **97**, 054105 (2018).

[77] X. Ni, H. Huang, and F. Liu, Phys. Rev. B **101**, 125114 (2020).

[78] B. Focassio, G. R. Schleder, M. Costa, A. Fazzio, and C. Lewenkopf, 2D Mater. **8**, 025032 (2021).

[79] B. R. K. Nanda, M. Sherafati, Z. S. Popović, and S. Satpathy, New J. Phys. **14**, 083004 (2012).

[80] S. Atkinson, G. Zhang, A. B. Hopkins, and S. Torquato, Phys. Rev. E **94**, 012902 (2016).